Biochemical and Biophysical Research Communications 498 (2018) 313–318

Contents lists available at ScienceDirect

Biochemical and Biophysical Research Communications

journal homepage: www.elsevier.com/locate/ybbrc

Molecular dynamics simulations of stratum corneum lipid mixtures: A multiscale perspective

Timothy C. Moore [a, b], Christopher R. Iacovella [a, b], Anne C. Leonhard [a, b], Annette L. Bunge [c], Clare McCabe [a, b, d, *]

[a] Department of Chemical and Biomolecular Engineering, Vanderbilt University, Nashville, TN 37235, United States
[b] Vanderbilt University Multiscale Modeling and Simulation Center, Nashville, TN 37235, United States
[c] Department of Chemical and Biological Engineering, Colorado School of Mines, Golden, CO 80401, United States
[d] Department of Chemistry, Vanderbilt University, Nashville, TN 37235, United States

ARTICLE INFO

Article history:
Received 13 July 2017
Received in revised form
4 September 2017
Accepted 8 September 2017
Available online 11 September 2017

Keywords:
Multistate iterative Boltzmann inversion
Coarse-grained
Ceramide
Self-assembly
Skin

ABSTRACT

The lipid matrix of the stratum corneum (SC) layer of skin is essential for human survival; it acts as a barrier to prevent rapid dehydration while keeping potentially hazardous material outside the body. While the composition of the SC lipid matrix is known, the molecular-level details of its organization are difficult to infer experimentally, hindering the discovery of structure-property relationships. To this end, molecular dynamics simulations, which give molecular-level resolution, have begun to play an increasingly important role in understanding these relationships. However, most simulation studies of SC lipids have focused on preassembled bilayer configurations, which, owing to the slow dynamics of the lipids, may influence the final structure and hence the calculated properties. Self-assembled structures would avoid this dependence on the initial configuration, however, the size and length scales involved make self-assembly impractical to study with atomistic models. Here, we report on the development of coarse-grained models of SC lipids designed to study self-assembly. Building on previous work, we present the interactions between the headgroups of ceramide and free fatty acid developed using the multistate iterative Boltzmann inversion method. Validation of the new interactions is performed with simulations of preassembled bilayers and good agreement between the atomistic and coarse-grained models is found for structural properties. The self-assembly of mixtures of ceramide and free fatty acid is investigated and both bilayer and multilayer structures are found to form. This work therefore represents a necessary step in studying SC lipid systems on multiple time and length scales.

1. Introduction

Skin plays the essential role in human physiology of preventing water loss and protecting the body form external physical, chemical and biological attack. This barrier function is known to be localized to the stratum corneum (SC), the outermost layer of skin [1]. The SC is composed of dead skin cells surrounded by a dense lamellar-structured lipid matrix containing an approximately equimolar mixture of ceramides (CERs), free fatty acids (FFAs), and cholesterol [2]. This lipid mixture notably lacks phospholipids, which are present in most biological membranes. Since the lipid matrix is the only continuous path through the SC, it is generally recognized that the lipids play an integral role in the barrier properties of skin. Anomalies in lipid composition are known to be associated with impaired barrier function, (see, for example, Refs. [3–6]); however, while many global properties of SC lipid systems can be gleaned from experimental measurements, molecular-level details often remain elusive. Hence, atomistic molecular dynamics simulations have begun to play an important role in examining the molecular-level structure and composition-related changes to membrane structure and properties [7–15], typically focusing on systems based on CER NS (C18 sphingosine base linked to a non-alpha hydroxy acyl chain). Simulation studies have thus far provided considerable insight into the role of CER acyl chain length [12,16], CER headgroup chemistry [11], and the addition of other lipids on bilayer properties [9,13,15–17], as well as examining the permeation of small molecules through CER based bilayers [12,18,19].

* Corresponding author. Department of Chemical and Biomolecular Engineering, Vanderbilt University, Nashville, TN 37235, United States.
E-mail address: c.mccabe@vanderbilt.edu (C. McCabe).

http://dx.doi.org/10.1016/j.bbrc.2017.09.040
0006-291X/

However, most studies have relied on preassembled bilayer configurations, which may unduly influence the resulting structure and observed properties; the dense, gel phase structures formed by the SC lipids result in very low lipid mobility [14], making them effectively stuck in their initial configurations over the typical simulation timescales considered. The use of bilayer, rather than multilayer structures, may also limit the insight that can be gained, as they restrict the conformations that can be adopted for the two-tailed CERs, e.g., hairpin versus extended, which is a controversial topic in the experimental literature [20]. Self-assembled structures, where lipids form the desired structure with minimal external input, would be preferable, but the timescales required to reach equilibrium on what is likely a rough free energy landscape make this approach impractical for atomistic models.

To address these issues, computationally efficient coarse-grained (CG) models can be used. CG models allow the long times and large systems sizes required to observe significant lipid rearrangements, including self-assembly, to be studied [21]. While numerous methods are available for deriving CG force fields [22–25], the structure-based iterative Boltzmann inversion (IBI) [26] method is commonly used. The IBI method iteratively updates pair potentials between successive CG simulations to match target data in the form of site-site radial distribution functions (RDFs), and has been successfully applied to systems ranging from small molecules [27] to lipids [28,29] and polymers [30–32]. While IBI yields force fields that generally reproduce the target fluid structure with high accuracy, these force fields often fail to reproduce behavior at other state points [27,31–33], as IBI only provides a means to match the target RDFs and cannot determine if the derived pair potentials accurately represent the underlying energy landscape. This problem is further intensified by the fact that there may be any number of pair potentials that sufficiently reproduce the target RDF [33], and determination of which one is most representative is nontrivial. Hence, the utility of IBI-based force fields may be limited for studying processes that span multiple states, e.g., self-assembly.

In recent work, we developed a multistate extension to IBI (MS IBI) that helps to address the transferability problem of IBI-derived force fields, whereby pair potentials are optimized to match target RDFs at multiple state points simultaneously [33]. This extension effectively adds additional constraints to the optimization process, with the goal of finding a pair potential that simultaneously matches each target RDF, and thus adequately represents the underlying energy landscape. In this communication, we provide an overview of the MS IBI algorithm and summarize prior usage of this methodology to produce CG force fields that are more robust and transferable than single-state methods. We additionally expand on our prior study of SC lipids and present the derivation of the cross-interactions between FFA and CER NS headgroups, and use this force field to investigate the self-assembly of large membranes composed of mixtures of CER and FFA.

1.1. Background: MS IBI

As an extension of the IBI method (single state IBI, or SS IBI), MS IBI updates trial pair potentials based on the deviation between multiple target RDFs and RDFs from running a CG simulation using the trial pair potentials. Instead of a single update term, each state used in the optimization contributes to the update, given by

$$V_{\gamma\beta}^{(i+1)}(r) = V_{\gamma\beta}^{(i)}(r) - N_{states}^{-1} \sum_{states} \alpha_s(r)\, k_B\, T_s \ln\left[\frac{g_{\gamma\beta,s}^{AA}(r)}{g_{\gamma\beta,s}^{(i)}(r)}\right],$$

where $V_{\gamma\beta}^{(i)}(r)$ is the pair potential between bead types γ and β at the i^{th} iteration, N_{states} is the number of states used to optimize $V_{\gamma\beta}$, $\alpha_s(r)$ serves as a damping and weighting function, used to reduce the size of the potential updates and to adjust the "weight" given to each state, T_s is the temperature of state s, k_B is Boltzmann's constant, $g_{\gamma\beta,s}^{AA}(r)$ is the target $\gamma\beta$ RDF at state s, and $g_{\gamma\beta,s}^{(i)}(r)$ is the $\gamma\beta$ RDF calculated from a simulation of $V_{\gamma\beta}^{(i)}(r)$. In the limit of a single state, MS IBI reduces to the original SS IBI algorithm. Note that alpha is set to a linear function of the separation, with $\alpha(0) = \alpha_0$, and $\alpha(r_{cut}) = 0$; this allows larger updates to occur at short separations, which we found to help reduce structural artifacts in the resulting pair potentials. Additionally, α_s is allowed to vary by state, allowing certain states to be given a higher or lower weight, enabling certain behavior or structures to be emphasized [33]. While the goal of MS IBI is to derive a single transferable force field, this cannot necessarily be achieved in all cases, e.g., due to structural rearrangements at the sub-CG bead size scale (similar to how atomistic force fields may lack transferability if the electron density distribution is sufficiently different between states) and for extremely different target states [33]. Thus, adjustment of the relative weights can be used as a means to provide a desired compromise of RDF *fitness* (e.g., providing a better fit in the RDFs for the state point of most interest).

MS IBI has allowed the development of more robust force fields than the SS IBI approach. For example, using only bulk alkane RDFs, an MS IBI-derived force field was shown to accurately predict the structural properties of both gel and liquid crystalline monolayers, while SS IBI-derived force fields using the same targets failed to accurately capture the behavior of both monolayer states [33]. In other work, MS IBI was used to improve upon an existing CG water force field by using both bulk water and water droplet target states, enabling the resulting CG force field to accurately capture both structural correlations and surface tension [34]; a prior SS IBI-based water model [35] could reproduce structure but not surface tension. In recent work [37], a force field for CER NS was optimized against both lamellar and bulk fluid target states, finding close agreement with the structural properties of each state and in better agreement with experiment than the MARTINI-CER force field [36]. The MS-IBI derived CG force field was also shown to reproducibly self-assemble into ordered membrane structures [37]. The multistate nature of MS IBI also allows beads to be made transferable between different molecules by simultaneously using target data from different molecules that share common beads; e.g., the tail beads in FFA and CER NS are identical and thus optimization of the TAIL-TAIL pair potential included both FFA and CER NS target data. MS IBI has also been used to capture appropriate density-pressure relationships by performing multi-ensemble (e.g., NVT and NPT) optimizations for water and lipids [34,37]. We have additionally demonstrated coupling of the MS IBI optimizations with a simulated wetting procedure to address a particular shortcoming associated with structure-based force fields; that is, the underlying structure matching procedure cannot differentiate between correlations in the RDFs that result from density and those that result from an underlying attraction, making it difficult to accurately capture hydrophobic interactions. We demonstrated that the hydrophobicity of the lipid tail beads can be corrected by systematically reducing the tail-water attraction such that the contact angle of a water droplet on a monolayer surface composed of lipid tails in a CG simulation matched that from a corresponding atomistic simulation.

The rest of this Communication is organized as follows: the models and methods used to optimize the CER-FFA cross-interactions are detailed in Section 2. In Section 3, the results of the optimizations are presented and the self-assembly of CER-FFA

mixtures into lamellar structures explored. Finally, conclusions and a general outlook are briefly discussed in Section 4.

2. Methods and model

2.1. Simulations

Atomistic simulations used to gather target data were run with the CHARMM36 all-atom force field [38]. Parameters for the CER NS headgroups were taken from our previous work [11]; these have been shown to accurately reproduce the phase behavior of a pure CER NS bilayer. Water, when present, was modeled with TIP3P [39]. Bulk fluid mixtures and bilayers composed of CER NS and FFA were used to gather target data. Two classes of CG simulations were performed: those during the MS IBI optimizations and those using the optimized force field. Simulation- and analysis-specific details can be found in the Supplementary Material.

2.2. Model description and force field optimization

The coarse-grained mappings for the lipids used in this work are shown in Fig. 1 and were defined in a previous publication [37]. Briefly, a 3-to-1 mapping is used, where each CG bead generally represents 3 heavy atoms. A notable exception is the hydroxyl groups in the CER headgroup, which are each mapped to a single bead; this was found to be necessary to capture the in-plane packing of the CER headgroups in a bilayer configuration [37]. Both molecules share identical TAIL beads, which represent 3 successive carbons and their associated hydrogens in the lipid tails. A description of the various terms in the force field can be found in the Supplementary Material.

The bonded interactions and nonbonded pair potentials for beads on the same type of molecule, along with the lipid-water pair potentials, were optimized with MS IBI and reported in previous work [37]. In this work, we optimize the lipid-cross interactions, i.e., the AMIDE-HEAD, MHEAD2-HEAD, OH1-HEAD, and OH2-HEAD pair potentials, using MS IBI. Bilayer and bulk fluid states were used for these optimizations, and included a constant pressure and a constant volume bilayer state at the same density. Details pertaining to the optimizations can be found in the Supplementary Material.

3. Results and discussion

3.1. Force field derivation and validation

The results of the CER NS-FFA headgroup optimizations are shown in Fig. 2 for the NPT states and in the Supplementary Material for the NVT states. The target RDFs are reproduced with a high degree of accuracy at the bilayer states, as indicated by the f_{fit} values > 0.95. The first peak and the general shape of the RDFs are accurately reproduced for each pair, which indicates that the CG model accurately captures the structural ordering of the headgroups within the bilayer plane. The RDFs at the bulk states are also accurately captured, with $0.891 \leq f_{fit} \leq 0.915$ for all pairs. The CG model generally underpredicts the height of the first RDF peak slightly and overpredicts the RDF beyond the first peak, which indicates a higher degree of headgroup clustering but a lower degree of ordering in the first solvation shell in the CG model compared to the atomistic one. Note that the AMIDE-HEAD interactions for the bulk show the largest deviation, due to the anisotropic interactions, as seen in prior work [37]. The CG model has slightly longer-ranged ordering than the atomistic, which is a necessary compromise in order to capture the ordering in the bilayer states. The lower degree of RDF matching in the bulk phases is expected, as the bilayer states were given higher weight (via $\alpha_s(r)$), since they are ultimately of more interest. Despite the lower fitness in the bulk states, the bulk densities calculated via NPT simulations with the CG (0.713 ± 0.003 g/mL) and atomistic models (0.703 ± 0.006 g/mL) compare favorably.

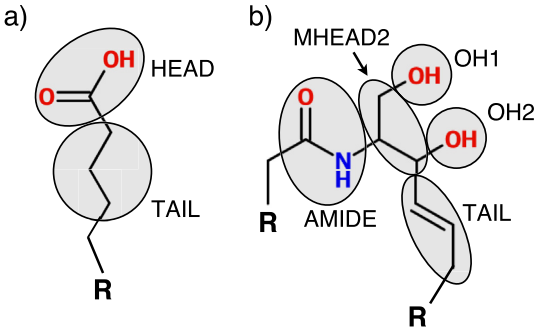

Fig. 1. CG mappings for the lipid headgroups considered in this work; a) FFA and b) CER NS. "R" represents a set of TAIL beads bonded in series, with the number of tail beads determined by length of the lipid tails. Note that the CG beads interact through spherically symmetric potentials despite being drawn as ellipses.

The pair potentials were further validated with a 200 ns simulation of the equimolar CER NS C24-FFA C24:0 bilayer to examine structural properties beyond the RDF, which are listed in Table 1. The high nematic order parameter (S_2) shows that both models form bilayers with a high degree of orientational order in the lipid tails. The CG model overpredicts the area per lipid (APL) by ~5%, which is of the same order as the deviation calculated for a pure CER NS C24 bilayer [37]. The atomistic model predicts a higher tilt angle of the lipid tails with respect to the bilayer normal, although the difference is quite small (~7% difference when considering the relevant scale of 0–90°). The bilayer thickness agrees very well with the atomistic model, differing by 1 Å, illustrating the structural accuracy of the model with regard to both the lipid tails and the lipid-water interface. Overall, we find excellent agreement in the structural properties of multicomponent bilayers simulated with the atomistic and CG models.

3.2. Self-assembly into lamellar structures

Next, the self-assembly of the CG model into lamellar structures that are completely decorrelated from the initial configuration is examined. In general, bilayer self-assembly occurs in two major steps [40]. First, the lipids aggregate in the water to form separate lipid and aqueous domains; next, the lipids organize themselves such that the hydrophilic headgroups shield the hydrophobic tails from the aqueous phase, thus forming a bilayer structure. In this work, we initialize the lipids in a high temperature, disordered, but phase-separated, configuration, shown in Fig. 3a; the systems were set up such that the lipid phase spans the box in the *x* and *y* directions, but not along *z*, to ensure that the lipids can form a 2D periodic structure. From the high temperature state, the system temperature was first reduced to 305 K over 100 ns, followed by an isochoric expansion in the *xy* plane to 1.7x the APL of the preassembled, equilibrated bilayer. The system was then isochorically compressed in the *xy* plane to the equilibrium bilayer APL, after which the semi-isotropic barostat was activated, and the simulation continued for another 200 ns at 305 K and 1 atm. This approach of starting from a phase-separated state, followed by expansion and compression, was found in prior work to not affect the self-assembled structures, but rather makes the self-assembly more efficient and reliable, as major structural defects are more rapidly worked out compared to simply simulating the system at a constant temperature and pressure [37]. Three different bilayer

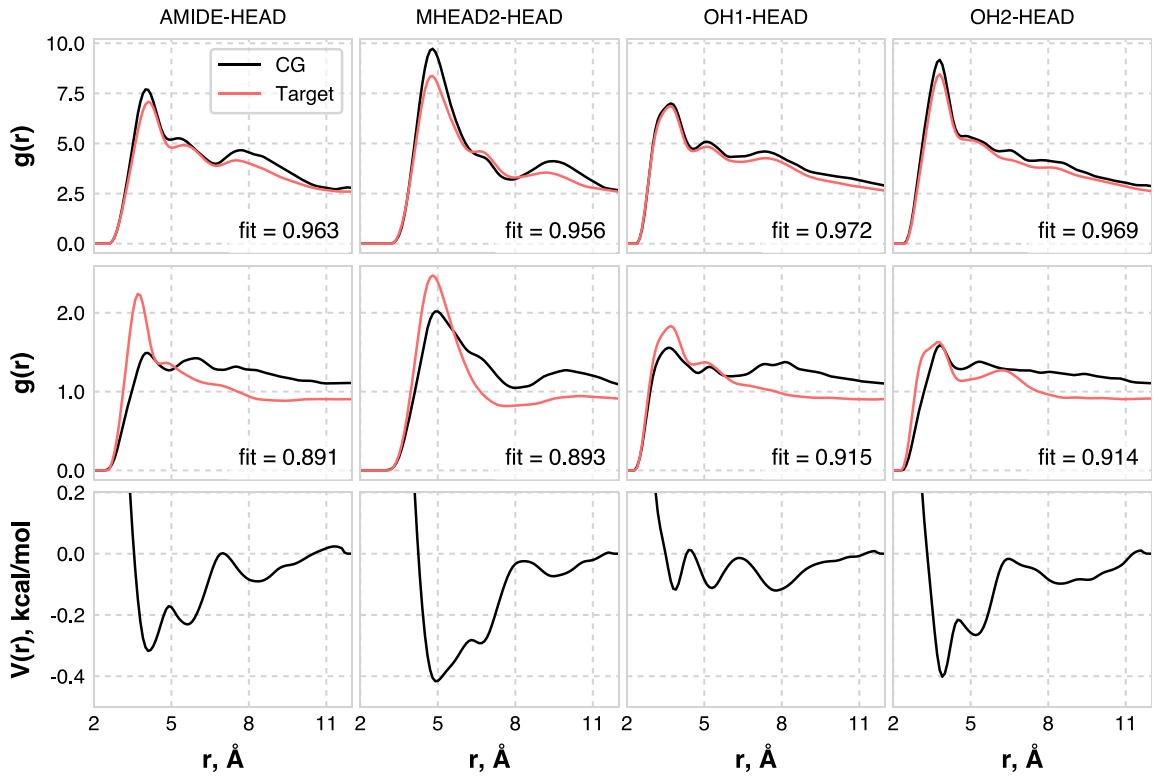

Fig. 2. Representative RDFs and final optimized pair potentials for the pair interactions considered in this work. Each column corresponds to a single pair, given at the top of the column. The first row shows the target and CG RDFs at the NPT bilayer state, the middle row shows the target and CG RDFs at the NPT bulk fluid state, and the bottom row shows the optimized pair potentials. The RDFs for the states not shown here are shown in the Supplementary Material.

Table 1
Comparison of structural properties of equimolar CER NS C24-FFA C24:0 preassembled (PA) and self-assembled (SA) bilayers simulated with the atomistic and CG models. The two numbers listed for the self-assembled systems (CG, SA-X) are for each of the two leaflets, as the asymmetric distribution of lipids between the leaflets, which is listed in the rightmost column, gives rise to different properties of the individual leaflets. Uncertainties represent the standard error in the calculations; for the self-assembled system, the uncertainties are on the same order as the preassembled CG system.

System	S_2	APL, Å^2	Tilt, deg	Thickness, Å	n_{top}:n_{bottom}
Atomistic, PA	0.991 ± 0.001	29.2 ± 0.4	13 ± 2	59.7 ± 0.1	–
CG, PA	0.9787 ± 8.7e-4	30.87 ± 0.07	6.3 ± 0.5	60.72 ± 0.02	–
CG, SA-1	0.964/0.975	31.18/30.68	9.6/6.1	60.22 ± 0.01	0.965
CG, SA-2	0.976/0.976	31.36/30.70	6.4/6.2	60.79 ± 0.002	0.978
CG, SA-3	0.975/0.957	30.43/32.37	6.0/11.7	60.04 ± 0.02	1.064

self-assembly simulations were performed and analyzed to show reproducibility, with total compression/expansion times of 200 ns, 400 ns, and 600 ns (Table 1).

Stable, well-ordered bilayers formed in each of the three self-assembly simulations. Snapshots of one of the systems during the self-assembly process are shown in Fig. 3. Due to the stochastic nature of lipid organization during the cooling phase, the bilayers demonstrate an asymmetric distribution of lipids between the two leaflets and this asymmetry leads to different leaflets having different structural properties. This information is summarized in Table 1 and shows that when a particular leaflet has a lower APL (i.e., more lipids, since the area is taken as the area of the simulation box), the lipid tails in that leaflet are more ordered and demonstrate a smaller tilt angle. In general, the structural properties of the self-assembled bilayers tend to agree well with those of the pre-assembled bilayer. To examine the APL of the different lipid species individually, a Voronoi tessellation of the lipid positions in the bilayer plane was constructed and APLs of 40 ± 8 Å^2 for CER NS and 30 ± 8 Å^2 for FFA were obtained. While the APL for FFA is smaller, as expected given it has a single tail, these values seem low for CER

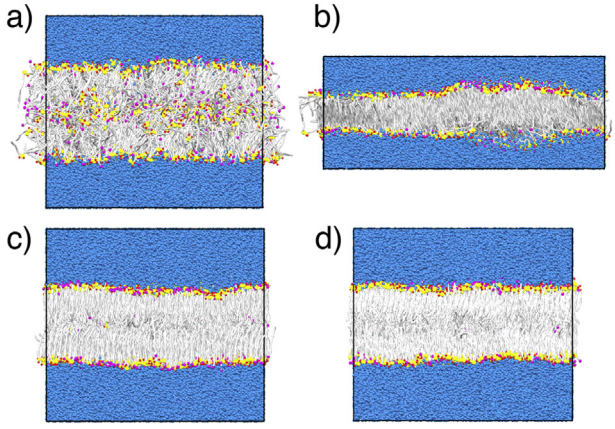

Fig. 3. System snapshots during the bilayer self-assembly process of an equimolar mixture of CER NS C24 and FFA C24:0: a) initial, disordered configuration, b) at maximum expansion, c) at the end of the compression phase, and d) after 200 ns of simulation at 305 K and 1 atm. CG beads are colored as follows: blue = water, silver = lipid tails, yellow = AMIDE and MHEAD2 beads, red = OH1 and OH2 beads, and magenta = FFA headgroups. (For interpretation of the references to colour in this figure legend, the reader is referred to the web version of this article.)

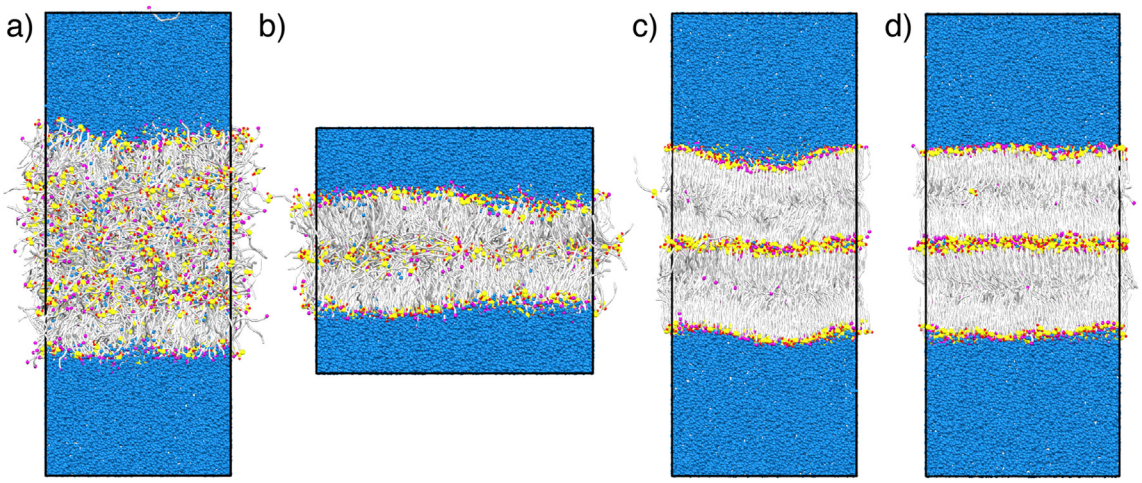

Fig. 4. Multilayer self-assembly process of an equimolar mixture of CER NS C24 and FFA C24:0: a) disordered configuration after resizing to fit two bilayers, b) at maximum expansion, c) the final configuration of the compression phase, and d) final configuration after 200 ns of simulation at 305 K and 1 atm. CG beads colored the same as in Fig. 3.(For interpretation of the references to colour in this figure legend, the reader is referred to the web version of this article.)

and high for FFA, and may be a result of the lipid headgroups being offset in the bilayer normal direction, as observed in previous work [41]. This offset is not captured when the headgroup positions are projected onto the same plane to construct the Voronoi tessellation (see the Supplementary Material for more details).

In the SC, the lipids are organized into repeating lamellar structures (i.e., multilayers), and thus understanding the lipid structure in multilayers is of considerable interest. Here, using the validated CG force fields, simulations of multilayer self-assembly were performed in a similar manner to the bilayer self-assembly simulations, with two changes. First, instead of initially cooling to 305 K from the initial configuration, the system is isochorically compressed in the *xy* plane to ½ the equilibrium bilayer APL, so that, in principle, two bilayers can fit within the simulation box. This compression was followed by the expansion/compression process used for bilayer self-assembly, except that the temperature was held at 550 K during the expansion, and then lowered to 305 K during the compression. The temperature was kept elevated to give the lipids more energy to reorganize during the expansion. To show reproducibility, three different total expansion/compression times were used: 200 ns, 400 ns, and 600 ns. Stable multilayer structures formed in each simulation. A representative self-assembly process is shown in Fig. 4. Of particular interest in these systems are the fractions of CER molecules that are in hairpin versus extended conformations, as this may have implications for the lamellar arrangements of CERs in the SC [20]. Here, we define an extended conformation as a CER where the angle between the two tails is greater than 90° and a hairpin conformation otherwise. In each of the self-assembled structures, between 23 and 28% of the CERs in the middle layers adopt a hairpin conformation, compared to 15% for pure CER systems [37], suggesting that a mixture of hairpin and extended conformations is favorable. All systems contain a thin layer of water mixed with the headgroups in the middle of the lipid phase, ranging from 0.127 to 0.221 water *beads* per lipid, corresponding to 0.508 to 0.884 water *molecules* per lipid, which is consistent with experimental observations of low lipid headgroup hydration in model SC membranes [42,43].

4. Conclusion and outlook

This work highlights the use of multiscale modeling in studying the SC layer of skin. While atomistic simulations can be used to study properties at the atomistic level, e.g., hydrogen bonding [11], CG models are needed to study systems on a larger scale. Building on prior work, here we use MS IBI to derive transferable CG models for skin lipids from atomistic simulations. These CG models can be used to study native lipid structures in the skin through self-assembly, which removes the influence of the initial configurations and hence the structures represent preferred lipid morphologies. As such, skin lipid systems can be computationally studied at multiple levels of resolution to provide a complete picture of how atomic-level features of lipids give rise to mesoscale properties. Information gleaned from these studies will prove useful for a wide range of applications, from strategies for restoring an impaired skin barrier to selectively penetrating the skin barrier, e.g., for transdermal drug delivery [44,45].

Acknowledgements

Funding: This work was supported by the National Institute of Arthritis and Musculoskeletal and Skin Diseases [grant number R01 AR057886-01]; the National Science Foundation [grant number CBET-1028374]; the National Energy Research Scientific Computing Center, supported by the Office of Science of the Department of Energy [contract number DE-AC02-05CH11231]; and the Advanced Computing Center for Research and Education at Vanderbilt University. AL acknowledges support from the National Science Foundation through grant number DMR-1560414.

Transparency document

Transparency document related to this article can be found online at http://dx.doi.org/10.1016/j.bbrc.2017.09.040.

Appendix A. Supplementary data

Supplementary data related to this article can be found at http://dx.doi.org/10.1016/j.bbrc.2017.09.040.

References

[1] P.W. Wertz, B. van den Bergh, The physical, chemical and functional properties of lipids in the skin and other biological barriers, Chem. Phys. Lipids 91 (1998) 85–96.
[2] K.C. Madison, Barrier function of the skin: "La raison d'Etre" of the epidermis,

J. Investigative Dermatology 121 (2003) 231–241.
[3] M. Janssens, J. van Smeden, G.S. Gooris, W. Bras, G. Portale, P.J. Caspers, R.J. Vreeken, T. Hankemeier, S. Kezic, R. Wolterbeek, A.P.M. Lavrijsen, J.A. Bouwstra, Increase in short-chain ceramides correlates with an altered lipid organization and decreased barrier function in atopic eczema patients, J. Lipid Res. 53 (2012) 2755–2766.
[4] A.P.M. Lavrijsen, J.A. Bouwstra, G.S. Gooris, A. Weerheim, H.E. Bodde, M. Ponec, Reduced skin barrier function parallels abnormal stratum corneum lipid organization in patients with lamellar ichthyosis, J. Investigative Dermatology 105 (1995) 619–624.
[5] G.S.K. Pilgram, D.C. Vissers, H. van der Meulen, S. Pavel, A.P.M. Lavrijsen, J.A. Bouwstra, H.K. Koerten, Aberrant lipid organization in stratum corneum of patients with atopic dermatitis and lamellar ichthyosis, J. Investigative Dermatology 117 (2001) 710–717.
[6] J. van Smeden, M. Janssens, W.A. Boiten, V. van Drongelen, L. Furio, R.J. Vreeken, A. Hovnanian, J.A. Bouwstra, Intercellular skin barrier lipid composition and organization in Netherton syndrome patients, J. Investigative Dermatology 134 (2014) 1238–1245.
[7] S.A. Pandit, H.L. Scott, Molecular-dynamics simulation of a ceramide bilayer, J. Chem. Phys. 124 (2006), 14708–14708.
[8] C. Das, M.G. Noro, P.D. Olmsted, Fast cholesterol flip-flop and lack of swelling in skin lipid multilayers, Soft Matter 10 (2014) 7346–7352.
[9] C. Das, M.G. Noro, P.D. Olmsted, Simulation studies of stratum corneum lipid mixtures, Biophysical J. 97 (2009) 1941–1951.
[10] C. Das, M.G. Noro, P.D. Olmsted, Lamellar and Inverse Micellar Structures of skin lipids: effect of templating, Phys. Rev. Lett. 111 (2013), 148101–148101.
[11] S. Guo, T.C. Moore, C.R. Iacovella, L.A. Strickland, C. McCabe, Simulation study of the structure and phase behavior of ceramide bilayers and the role of lipid head group chemistry, J. Chem. Theory Comput. 9 (2013) 5116–5126.
[12] R. Gupta, B.S. Dwadasi, B. Rai, Molecular dynamics simulation of skin lipids: effect of ceramide chain lengths bilayer properties, J. Phys. Chem. B 120 (2016) 12536–12546.
[13] R. Gupta, B. Rai, Molecular dynamics simulation study of skin lipids: effects of the molar ratio of individual components over a wide temperature range, J. Phys. Chem. B 119 (2015) 11643–11655.
[14] M.I. Hoopes, M.G. Noro, M.L. Longo, R. Faller, Bilayer structure and lipid dynamics in a model stratum corneum with oleic acid, J. Phys. Chem. B 115 (2011) 3164–3171.
[15] R. Notman, W.K. den Otter, M.G. Noro, W.J. Briels, J. Anwar, The permeability enhancing mechanism of DMSO in ceramide bilayers simulated by molecular dynamics, Biophysical J. 93 (2007) 2056–2068.
[16] C. Das, P.D. Olmsted, The physics of stratum corneum lipid membranes, Philosophical Trans. R. Soc. A 374 (2016) 20150126.
[17] A. Akinshina, C. Das, M.G. Noro, Effect of monoglycerides and fatty acids on a ceramide bilayer, Phys. Chem. Chem. Phys. 18 (2016) 17446–17460.
[18] C. Das, P.D. Olmsted, M.G. Noro, Water permeation through stratum corneum lipid bilayers from atomistic simulations, Soft Matter 5 (2009), 4549–4549.
[19] R. Gupta, B.S. Dwadasi, B. Rai, Molecular dynamics simulation study of permeation of molecules thorough skin lipid bilayers, J. Phys. Chem. B 120 (2016) 8987–8996.
[20] D. Kessner, A. Ruettinger, M.A. Kiselev, S. Wartewig, R.H.H. Neubert, Properties of ceramides and their impact on the stratum corneum structure. Part 2: stratum corneum lipid model systems, Skin Pharmacol. Physiology 21 (2008) 58–74.
[21] H.I. Ingolfsson, C.A. Lopez, J.J. Uusitalo, D.H. de Jong, S.M. Gopal, X. Periole, S.J. Marrink, The power of coarse graining in biomolecular simulations, Wiley Interdisciplinary Reviews, Comput. Mol. Sci. 4 (2014) 225–248.
[22] F. Ercolessi, J.B. Adams, Interatomic potentials from first-principles calculations: the force matching method, Europhys. Lett. (EPL) 26 (1994) 583–588.
[23] S. Izvekov, G.A. Voth, A multiscale coarse-graining method for biomolecular systems, J. Phys. Chem. B 109 (2005) 2469–2473.
[24] A.P. Lyubartsev, A. Laaksonen, Calculation of effective interaction potentials from radial distribution functions: a reverse Monte Carlo approach, Phys. Rev. E 52 (1995) 3730–3737.
[25] A. Chaimovich, M.S. Shell, Coarse-graining errors and numerical optimization using a relative entropy framework, J. Chem. Phys. 134 (2011), 094112–094112.
[26] D. Reith, M. Putz, F. Müller-Plathe, Deriving effective mesoscale potentials from atomistic simulations, J. Comput. Chem. 24 (2003) 1624–1636.
[27] H.-j. Qian, P. Carbone, X. Chen, H.A. Karimi-varzaneh, C.C. Liew, F. Müller-Plathe, Temperature-transferable coarse-grained potentials for ethylbenzene, polystyrene, and their mixtures, Macromolecules 41 (2008) 9919–9929.
[28] K.R. Hadley, C. McCabe, A structurally relevant coarse-grained model for cholesterol, Biophysical J. 99 (2010) 2896–2905.
[29] K.R. Hadley, C. McCabe, A coarse-grained model for amorphous and crystalline fatty acids, J. Chem. Phys. 132 (2010), 134505–134505.
[30] R. Faller, D. Reith, Properties of poly(isoprene): model building in the melt and in solution, Macromolecules 36 (2003) 5406–5414.
[31] B. Bayramoglu, R. Faller, Coarse-grained modeling of polystyrene in various environments by iterative Boltzmann inversion, Macromolecules 45 (2012) 9205–9219.
[32] B. Bayramoglu, R. Faller, Modeling of polystyrene under confinement: exploring the limits of iterative Boltzmann inversion, Macromolecules 46 (2013) 7957–7976.
[33] T.C. Moore, C.R. Iacovella, C. McCabe, Derivation of coarse-grained potentials via multistate iterative Boltzmann inversion, J. Chem. Phys. 140 (2014), 224104–224104.
[34] T.C. Moore, C.R. Iacovella, C. McCabe, in: R.Q. Snurr, C.S. Adjiman, D.A. Kofke (Eds.), Development of a coarse-grained water forcefield via multistate iterative Boltzmann inversion, Springer, Singapore, 2016, pp. 37–52.
[35] K.R. Hadley, C. McCabe, On the investigation of coarse-grained models for water: balancing computational efficiency and the retention of structural properties, J. Phys. Chem. B 114 (2010) 4590–4599.
[36] Ž. Sovová, K. Berka, M. Otyepka, P. Jurečka, Coarse-grain simulations of skin ceramide ns with newly derived parameters clarify structure of melted phase, J. Phys. Chem. B 119 (2015) 3988–3998.
[37] T.C. Moore, C.R. Iacovella, R. Hartkamp, A.L. Bunge, C. McCabe, A coarse-grained model of stratum corneum lipids: free fatty acids and ceramide ns, J. Phys. Chem. B 120 (2016) 9944–9958.
[38] J.B. Klauda, R.M. Venable, J.A. Freites, J.W. O'Connor, D.J. Tobias, C. Mondragon-Ramirez, I. Vorobyov, A.D. MacKerell, R.W. Pastor, Update of the CHARMM all-atom additive force field for lipids: validation on six lipid types, J. Phys. Chem. B 114 (2010) 7830–7843.
[39] W.L. Jorgensen, J. Chandrasekhar, J.D. Madura, R.W. Impey, M.L. Klein, Comparison of simple potential functions for simulating liquid water, J. Chem. Phys. 79 (1983), 926–926.
[40] S.J. Marrink, E. Lindahl, O. Edholm, A.E. Mark, Simulation of the spontaneous aggregation of phospholipids into bilayers, J. Am. Chem. Soc. 123 (2001) 8638–8639.
[41] R. Hartkamp, T.C. Moore, C.R. Iacovella, M.A. Thompson, P. Bulsara, D.J. Moore, C. McCabe, Investigating the structure of multicomponent gel phase lipid bilayers, Biophysical J. 111 (2016) 813–823.
[42] M.A. Kiselev, N.Y. Ryabova, A.M. Balagurov, S. Dante, T. Hauß, J. Zbytovská, S. Wartewig, R.H.H. Neubert, New insights into the structure and hydration of a stratum corneum lipid model membrane by neutron diffraction, Eur. Biophysics J. 34 (2005) 1030–1040.
[43] T.N. Engelbrecht, A. Schröter, T. Hauß, B. Demé, H.A. Scheidt, D. Huster, R.H.H. Neubert, The impact of ceramides NP and AP on the nanostructure of stratum corneum lipid bilayer. Part I: neutron diffraction and 2H NMR studies on multilamellar models based on ceramides with symmetric alkyl chain length distribution, Soft Matter 8 (2012) 6599–6607.
[44] R.H. Guy, Transdermal drug delivery, in: M. Schaefer-Korting (Ed.), Drug Delivery, Springer, Berlin Heidelberg, 2010, pp. 399–410.
[45] M.R. Prausnitz, R. Langer, Transdermal drug delivery, Nat. Biotechnol. 26 (2008) 1261–1268.

Supplementary Material for "Molecular Dynamics Simulations of Stratum Corneum Lipid Mixtures: A Multiscale Perspective"

Timothy C. Moore,[a,b] Christopher R. Iacovella,[a,b] Anne Leonhard,[a,b] Annette L. Bunge,[c] and Clare McCabe[a,b,d,*]

[a]*Department of Chemical and Biomolecular Engineering, Vanderbilt University, Nashville, TN 37235, United Stated*

[b]*Vanderbilt University Multiscale Modeling and Simulation Center, Nashville, TN 37235, United States*

[c]*Department of Chemical and Biological Engineering, Colorado School of Mines, Golden, CO 80401, United States*

[d]*Department of Chemistry, Vanderbilt University, Nashville, TN 37235, United States*

**Corresponding author: c.mccabe@vanderbilt.edu*

Atomistic Simulation Details

For the atomistic simulations using the CHARMM36 force field, vdW interactions were neglected beyond 12 Å, and were set to smoothly decay to zero between 10 and 12 Å. Long-ranged electrostatic interactions were treated with the particle mesh Ewald method [1] with a real-space cutoff of 12 Å. All atomistic simulations were run with GROMACS 5.1 [2] with a 1 fs timestep. Constant pressure simulations of bulk fluid states employed an isotropic barostat, while bilayer states employed a semi-isotropic barostat with the pressure controlled independently in the bilayer normal and lateral directions. In both cases, the barostat used a pressure coupling constant of 10 ps and a compressibility of 4.5E-5 bar^{-1}.

Three distinct atomistic simulations were performed. First a bulk fluid equimolar mixture of CER NS C24 and FFA C24:0, with 100 molecules of each, at 1 atm and 500 K. 500 K was used to induce a fluid phase, as the lipids were found to be frozen at the skin temperature of 305 K. This system was initialized by placing the lipids on a lattice in a very large simulation box and simulating for 5 ns at 800 K, followed by slowly reducing the temperature to 500 K while compressing the system down to a realistic density over 5 ns. The barostat was then turned on and the system was allowed to equilibrate for 5 ns, followed by 10 ns of data collection. A corresponding system was run at constant volume, with the density set to the average density from the constant pressure simulation. The remaining atomistic simulation was a bilayer containing an equimolar mixture of CER NS C24 and FFA C24:0. The initialization and equilibration of this system follows the protocol described in recent work [3]. Briefly, the system was equilibrated for a total of 150 ns using a simulated tempering algorithm, and then simulated for a further 50 ns over which target data was collected.

Description of Coarse-Grained Force Field

CG beads are considered bonded if any two atoms represented by the two CG beads share a bond in the atomistic model. CG beads that are bonded interact through a harmonic bond-stretching potential, and any consecutively bonded triplet of CG beads interact through a harmonic angle-bending potential; the derivation of the parameters for these interactions follows the method of Milano et al. [4]. We note that we increased the TAIL-TAIL-TAIL angle constant from 6.33 kcal/mol to 56.97 kcal/mol in this work; this was not found to influence the properties of the systems investigated here, but was found to be necessary in preliminary work when considering molecules that act as fluidizing agents (e.g., cholesterol). In addition to the bonded interactions, CG beads also interact through nonbonded pair potentials, which were optimized with MS IBI. Note that the nonbonded pair interactions are neglected for beads that interact through bonded potentials. The tabular nonbonded pair potential files and parameters for the bonded interactions can be found at https://github.com/iModels/sc-ff.

MS IBI Optimizations

Whilst optimizing the nonbonded pair potentials We set $\alpha_0 = 0.5$ for the bilayer states and $\alpha_0 = 0.1$ for the bulk states to place more emphasis on the bilayer behavior. The initial potentials were the Boltzmann-inverted RDFs from the bilayer state, i.e.,

$$V^0_{\gamma\beta}(r) = -k_B T \ln g^{(AA)}_{\gamma\beta,bilayer}(r).$$

The optimizations were terminated when the fitness function, defined as

$$f_{fit} = 1 - \frac{\int_0^{r_{cut}} \mathrm{d}r \left| g^{(i)}(r) - g^{(AA)}(r) \right|}{\int_0^{r_{cut}} \mathrm{d}r \left| g^{(i)}(r) \right| + \left| g^{(AA)}(r) \right|},$$

increased by less than 0.01 for each pair at each state. The optimizations were performed using the open source MSIBI python package, which is hosted at https://github.com/mosdef-hub/msibi.

CG Simulation Details

Initial configurations for the MS IBI simulations were the final configurations from the corresponding atomistic simulations, mapped to the CG level. To increase sampling, bulk fluid CG systems were replicated 2x in each direction, and the bilayers were replicated 3x in each lateral direction. The bulk systems were run for 5 ns of equilibration, followed by 5 ns of data collection; the barostat was turned on in the final 1 ns of equilibration for the NPT state. The bilayer systems were equilibrated for 10 ns (with the barostat for the final 5 ns for the NPT state), followed by 30 ns of data collection. The pressure coupling scheme for the CG simulations was identical to the corresponding atomistic simulations, i.e., isotropic for the bulk systems and semi-isotropic for the bilayer systems. For force field validation, the initial configuration of the preassembled bilayer was the same as for the MS IBI CG simulations. The self-assembly simulations used several unique protocols, which are described in the corresponding sections in the main text. All CG simulations were run using the GPU-accelerated HOOMD-Blue toolkit [5, 6] with a 10 fs timestep.

Analysis

To quantify the structure of the bilayers, we calculated the area per lipid (APL), nematic order parameter and tilt angle of the lipid tails, and the bilayer thickness. These calculations are detailed in the SI of Ref. [7]. Importantly, we note that we first map the atomistic trajectories to the CG level to enable a more direct comparison with the CG simulations. For the self-assembled systems, we also quantify the asymmetry of the number of lipids in each leaflet. A lipid is considered in the top leaflet if the z component of its center of mass is greater than the z component of the total lipid center of mass, and in the bottom leaflet otherwise. This quantity was found to not fluctuate once the bilayers had formed. For information on the APL of each lipid species, we used a Voronoi

tessellation. The "generating points" of the tessellation were taken to be the positions of the HEAD beads (for FFA) and MHEAD2 beads (for CER). The Voronoi tessellation was performed with the pyvoro python package, which is a Python wrapper around the voro++ library (http://math.lbl.gov/voro++/) and is hosted at https://github.com/joe-jordan/pyvoro. Each cell was characterized by the species of its generating point (either CER or FFA); and the APL of each species was taken as the average area of each of that species' cells. A typical snapshot of a Voronoi tessellation is shown in Figure S1 below.

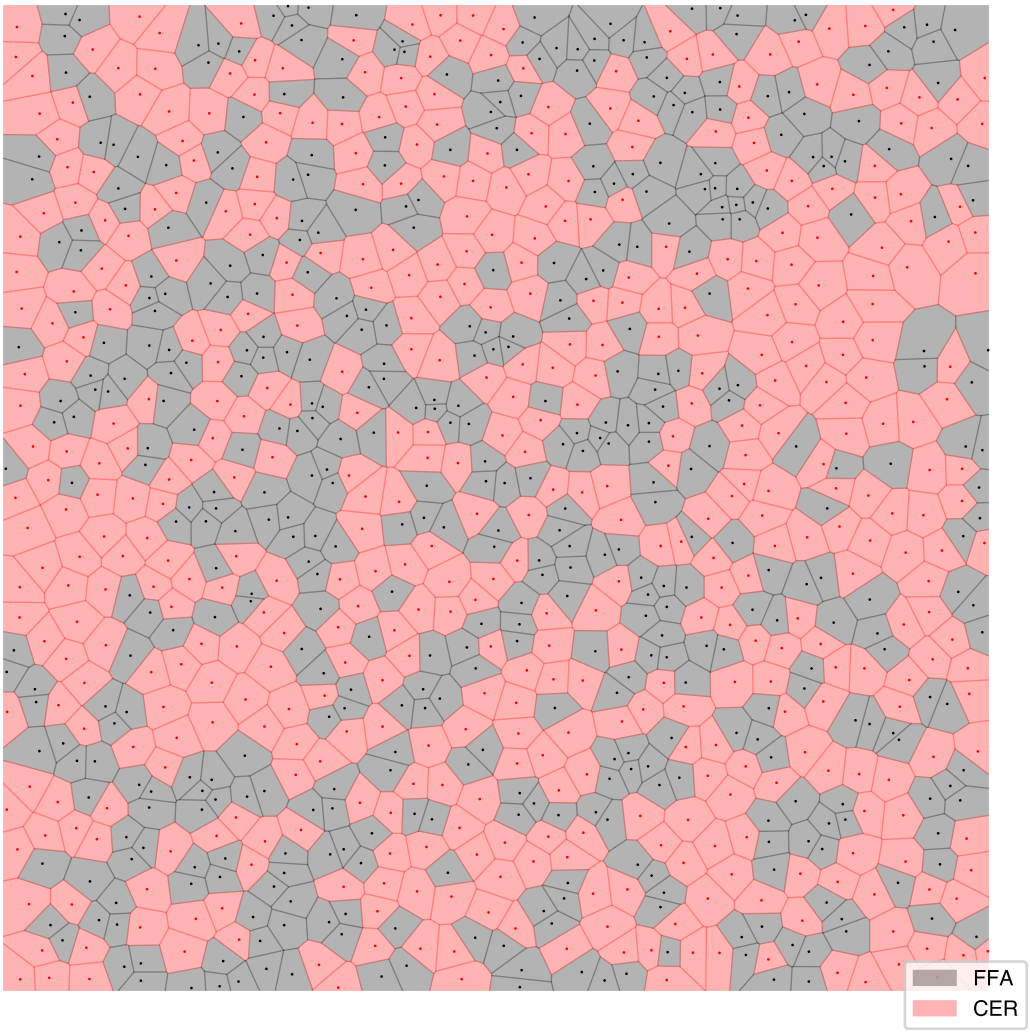

Figure S1. A typical Voronoi tessellation for a single bilayer leaflet. The location of the lipid headgroup within each cell is given by the point in that cell.

Voronoi Tessellation-Based Area per Lipid

The APL of the different lipid species was found to be 40 ± 8 Å^2 and 30 ± 8 Å^2 for CER and FFA, respectively. We make two observations about these results; first, the uncertainty is quite large for both, suggesting that the lipids do not have a well-defined cross-sectional area. Second, the values

are close to one another, especially when considering the uncertainty. However, these results may be affected by the distribution of headgroup positions along the bilayer normal direction. The Voronoi-based analysis relies on the headgroups residing in a common *z* plane; however, the lipid headgroups are somewhat offset in the bilayer normal direction. This offset in the *z* direction can lead to apparent overlaps when the headgroups are projected into a common *z* plane, which will affect the results of the calculation. Therefore, caution must be taken when interpreting these results.

RDFs from NVT States During MS IBI

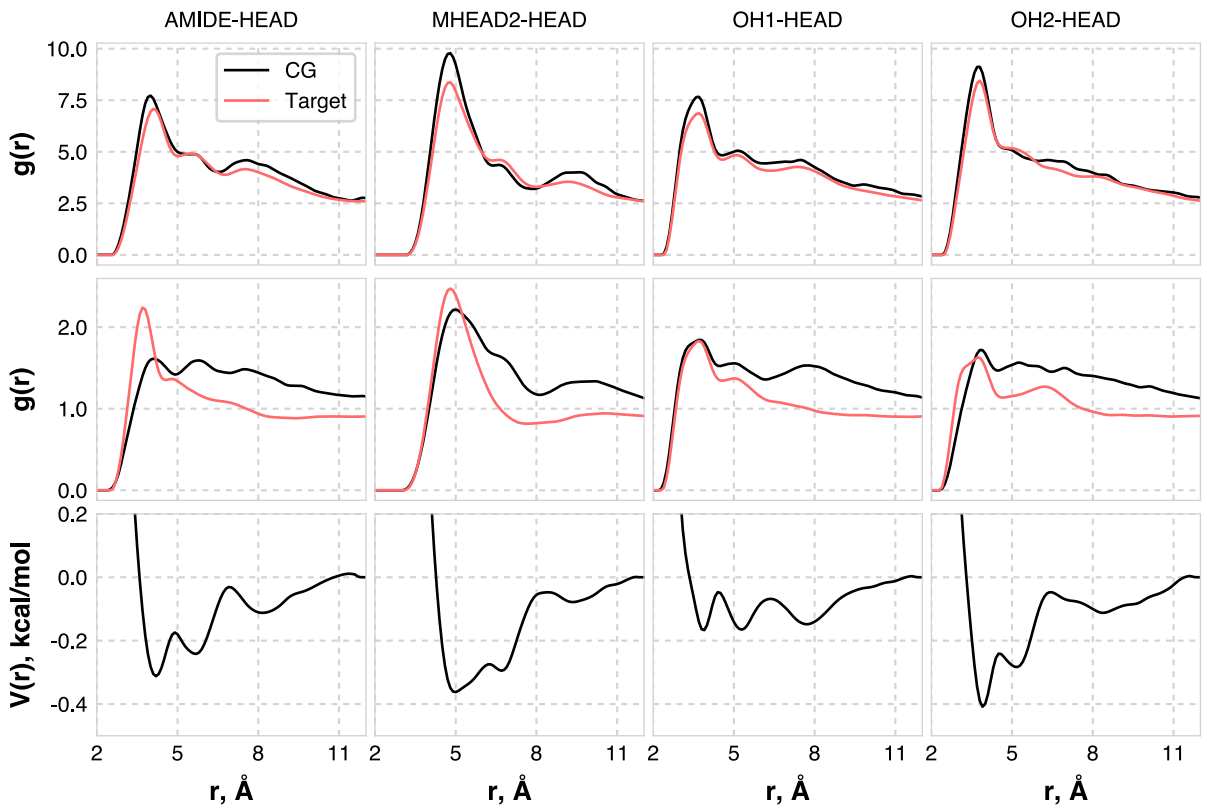

Figure S2. RDFs from the NVT states and final optimized pair potentials for the pair interactions considered in this work. Each column corresponds to a single pair, given at the top of the column. The first row shows the target and CG RDFs at the NVT bilayer state, the middle row shows the target and CG RDFs at the NVT bulk fluid state, and the bottom row shows the optimized pair potentials. Note that these pair potentials are the same as the ones shown in Fig. 2 in the main text and are provided here for reference.

References

[1] U. Essmann, L. Perera, M.L. Berkowitz, T. Darden, H. Lee, L.G. Pedersen, A smooth particle mesh Ewald method, The Journal of Chemical Physics, 103 (1995) 8577-8593.
[2] M.J. Abraham, T. Murtola, R. Schulz, S. Pall, J.C. Smith, B. Hess, E. Lindahl, Gromacs: High performance molecular simulations through multi-level parallelism from laptops to supercomputers, SoftwareX, 1-2 (2015) 19-25.
[3] T.C. Moore, R. Hartkamp, C.R. Iacovella, A.L. Bunge, C. McCabe, The Influence of Ceramide Tail Length on the Structure of Bilayers Composed of Stratum Corneum Lipids, submitted, 2017.
[4] G. Milano, S. Goudeau, F. Müller-Plathe, Multicentered Gaussian-based potentials for coarse-grained polymer simulations: Linking atomistic and mesoscopic scales, Journal of Polymer Science Part B: Polymer Physics, 43 (2005) 871-885.
[5] J.A. Anderson, C.D. Lorenz, A. Travesset, General purpose molecular dynamics simulations fully implemented on graphics processing units, Journal of Computational Physics, 227 (2008) 5342-5359.
[6] J. Glaser, T.D. Nguyen, J.A. Anderson, P. Lui, F. Spiga, J.A. Millan, D.C. Morse, S.C. Glotzer, Strong scaling of general-purpose molecular dynamics simulations on GPUs, Computer Physics Communications, 192 (2015) 97-107.
[7] T.C. Moore, C.R. Iacovella, R. Hartkamp, A.L. Bunge, C. McCabe, A Coarse-Grained Model of Stratum Corneum Lipids: Free Fatty Acids and Ceramide NS, The Journal of Physical Chemistry B, 120 (2016) 9944-9958.